CrossMark

In-vivo multi-exponential T2, magnetization transfer and quantitative histology in a rat model of intramyelinic edema[☆],[☆☆]

Kevin D. Harkins [a], William M. Valentine [b], Daniel F. Gochberg [a,c,d], Mark D. Does [a,c,e,f,*]

[a] Institute of Imaging Science, Vanderbilt University, USA
[b] Department of Pathology, Vanderbilt University, USA
[c] Department of Radiology and Radiological Sciences, Vanderbilt University, USA
[d] Department of Physics and Astronomy, Vanderbilt University, USA
[e] Department of Biomedical Engineering, Vanderbilt University, USA
[f] Department of Electrical Engineering, Vanderbilt University, USA

ARTICLE INFO

ABSTRACT

Two MRI methods, multi-exponential analysis of transverse relaxation (MET2) and quantitative magnetization transfer (qMT), were used along with quantitative evaluation of histology in a study of intra-myelinic edema in rat spinal white matter. The results showed a strong linear correlation between a distinct long-T2 signal from MET2 analysis and the edema water volume fraction as measured by histology, although this analysis overestimated the edema water content by $\approx 100\%$ relative to quantitative histological measurements. This overestimation was reasoned to result from the effects of inter-compartmental water exchange on observed transverse relaxation. Commonly studied MRI markers for myelin, the myelin water fraction (from MET2 analysis) and the macromolecular pool size ratio (from qMT analysis) produced results that could not be explained purely by changes in myelin content. The results demonstrate the potential for MET2 analysis as well as the limits of putative myelin markers for characterizing white matter abnormalities involving intra-myelinic edema.

1. Introduction

Many types of white matter lesions appear with high contrast in standard magnetic resonance imaging (MRI) protocols, however, the appearance of lesions is mostly unspecific for diagnosis. Both inflammation and demyelination will lead to an increase in average transverse relaxation time constant (T2) (Stanisz et al., 2004; Odrobina et al., 2005), thereby increasing contrast in a T2-weighted image. One example where the microstructural basis of T2 hyperintensity remains unclear is that seen in pediatric patients on the anti-seizure drug, vigabatrin. In several animal species, vigabatrin has been found to produce intra-myelinic edema (IME) (Cohen et al., 2000), which is characterized by a separation of the lamellae at the intraperiod line of compact myelin. In humans, vigabatrin has been associated with reversible T2 hyperintensity in pediatric patients (Dill et al., 2013; Dracopoulos et al., 2010; Pearl et al., 2009), but lack of imaging specificity has left the microanatomical basis for these observations unknown. Dracopoulos

et al. (2010) found a decrease in the apparent diffusion coefficient (ADC) of water corresponding to regions of T2 hyperintensity, which is consistent with IME (Karaarslan and Arslan, 2008; Righini et al., 2003), but Simao et al. (2011) found a directional dependence to the ADC change which led to the postulate that it resulted from axonal rather than myelinic sources. More recently, it has also been suggested that some observed T2 changes could correspond to physiologic rather than potentially pathologic changes (Aguilera-Albesa et al., 2012). From the perspective of MRI method development and evaluation, the unknown cause of T2 contrast observed in some patients taking vigabatrin is just one example of the need for establishing a stronger quantitative relationship between tissue microstructure and MRI contrast.

One approach for providing greater specificity to neuronal MRI contrast is through the use of multi-exponential T2 (MET2) analysis of water proton transverse relaxation, as measured through a multiple spin-echo imaging pulse sequence (Mackay et al., 1994). With this method, the water from within myelin, known as the myelin water fraction (MWF) has been distinguished from water in the intra- and extra-axonal spaces of white matter based on its short T2 (Laule et al., 2004; Mackay et al., 1994; Menon et al., 1992; Vasilescu et al., 1978). In addition to the MWF, the full spectrum of transverse relaxation time constants present in a tissue (hereafter, the T2 spectrum) provides other information about nervous system microstructure. For example, inflammation in the absence of myelin

loss shifts the long-T_2 components to greater T_2 values (Stanisz et al., 2004), and an additional long T_2 signal (>100 ms) has been observed in the white matter of patients with phenylketonuria (Laule et al., 2007; Sirrs et al., 2007) and in peripheral nerve exhibiting IME (Valentine et al., 2007). In contrast, the loss of myelin may result in a shift of the dominant T_2 component to longer times, as well as a decrease in the MWF (Does and Snyder, 1996; Odrobina et al., 2005; Stewart et al., 1993). Recent work in spinal white matter and nerve has also shown T_2-spectral sensitivity to microstructural dimensions, such as axon diameter and myelin thickness, through their effect on inter-compartmental water exchange (Dortch et al., in press; Dula et al., 2010; Harkins et al., 2012; Levesque and Pike, 2009; Sled et al., 2004). Thus, MET_2 offers a promising approach to characterizing nervous system abnormalities with greater microstructural specificity.

Another approach to providing micro-structural specificity to white matter MRI is through quantitative magnetization transfer (qMT) imaging (Gochberg and Gore, 2007; Sled and Pike, 2001; Yarnykh, 2002). This approach attempts to estimate the relative concentration of macromolecular protons through the exchange of magnetization between these protons and water. Because of the relatively high concentration of phospholipids and proteins in myelin compared to both intra- and extra-axonal spaces, an observed reduction of macromolecular pool size by qMT is reasoned to reflect a loss of myelin (Kucharczyk et al., 1994; Ou et al., 2009; Stanisz et al., 2001; Tozer et al., 2005). However, qMT may be less informative about microstructure than MET_2 when myelin content does not change (Dula et al., 2010; Levesque and Pike, 2009).

Given recent developments that make robust measurement of the MET_2 (Guo et al., in press; Lebel and Wilman, 2010; Prasloski et al., 2012a,b) relatively rapid and suitable for multi-slice or 3D acquisitions, and established clinically practical qMT methods (Sled and Pike, 2001; Smith et al., 2006; Yarnykh, 2002), further experimental studies that quantitatively evaluate the white matter microstructural changes that underlie T_2 and qMT contrast changes are warranted. This work reports evaluations of the specificity of MET_2 and qMT to IME induced by hexachlorophene (HCP) intoxication in rat spinal cord.

2. Materials and methods

2.1. Animals

Animal studies were completed in compliance with the Vanderbilt University Institutional Animal Care and Use Committee. Twenty-four female Sprague Dawley rats (pre-study weight 208–255 g) were split into three groups of 8 rats each and fed a diet containing various amounts of HCP, which is a toxin known to cause IME lesions histologically similar to those caused by vigabatrin (Graham, 1989). One group (referred to as HCP600) consumed a diet with 600 ppm HCP added to normal chow (TestDiet/LabDiet, Richmond, IN), another group (HCP300) consumed 300 ppm HCP, and a third group (CONTROL) consumed the same chow without added HCP. Doses were chosen to deliver approximately the same toxicity as 20 mg/kg/day and 40 mg/kg/day of HCP via oral gavage (Kennedy and Gordon, 1976), and similar to previous rat studies of HCP intoxication (Cammer et al., 1975; Kimbrough and Gaines, 1971; Lampert et al., 1973). All rats were held to the modified diet for four days prior to MR imaging, and the neurological status and weight of each rat were monitored daily. For all MRI studies, rats were anesthetized with isoflurane, respiration rate was continuously monitored, and a computer controlled external heater was used to maintain body temperature near 37 °C.

2.2. Magnetic resonance imaging

MR imaging was performed on a 9.4 T, 31-cm horizontal bore magnet with Varian/Agilent DirectDrive console (Santa Clara, CA)

using a 38-mm Litz quadrature coil (Doty Scientific, Columbia SC) for radiofrequency excitation and signal reception. From a sagittal scout image, a 1.5-mm thick slice was selected transverse to the long axis of the cervical spinal cord at the C2 level for further evaluation. Multi-exponential T_2 measurements were made using an inversion-recovery prepared multiple spin-echo imaging sequence as previously described (Harkins et al., 2012), with TR = 6 s. An initial 32 echoes were collected with a first echo time of 7.4 ms and an echo spacing of 9 ms, and final 8 echoes were collected with an echo spacing of 50 ms. Images were encoded with a 128×128 sampling over a 25.6×25.6 mm^2 field-of-view. The inversion-recovery preparation (inversion delay, TI = 2 s) was used to null signal from the cerebrospinal fluid, which otherwise caused significant motion-induced ghosting in long echo-time images. Signals from eight excitations were averaged resulting in an acquisition time ≈ 100 min. Quantitative magnetization transfer measurements were made with the same imaging geometry using a selective inversion-recovery prepared fast spin echo sequence (Gochberg and Gore, 2007) with a 1.5-ms hard inversion pulse, an echo train length of 16 and echo spacing of 5.6 ms. Images were acquired at 25 inversion times pseudo-logarithmically spaced between 3.5 ms and 10 s. The repetition pre-delay was fixed at 3.5 s and two signals were averaged resulting in an acquisition time ≈ 25 min. For both sequences, after $2 \times$ zero-padded reconstructions, the nominal in-plane resolutions were 100 μm in each direction.

All data analysis was performed using MATLAB (Mathworks, Natick, MA). Images were cropped to view the spinal cord, and regions of interest (ROIs) were drawn for each of four spinal white matter tracts: the dorsal cortical spinal tract (dCST), the funiculus gracilis (FG), the rubrospinal tract (RST) and the vestibulospinal tract (VST)
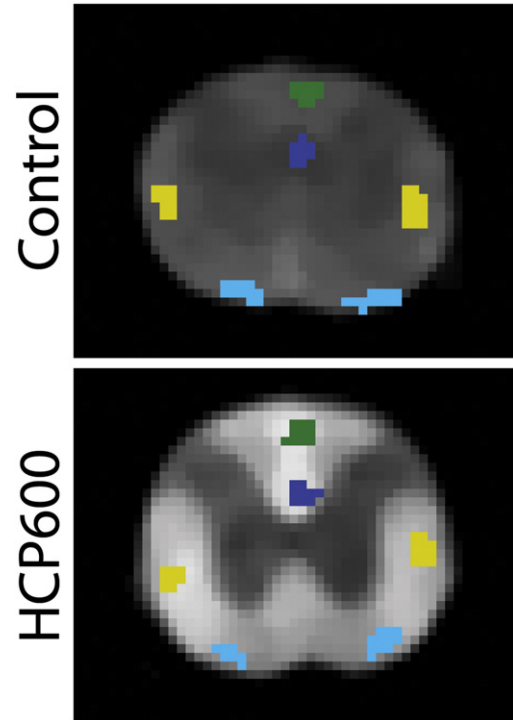
Fig. 1. Multi-exponential T_2 images from control and HCP600 rats at TE = 88.4 ms, showing hyperintensity in white matter regions of HCP intoxicated animals compared to controls. Example ROIs are shown for the dorsal cortical spinal tract (dCST, blue), the funiculus gracilis (FG, green), the rubrospinal tract (RST, yellow), and the vestibulospinal tract (VST, teal). Note that the relatively low white/gray contrast in the control spinal cord, which may be counterintuitive for a T_2-weighted image, is consistent with previous characterization of rat spinal cord (Carvlin et al., 1989; Narayana et al., 1999). Images were scaled to similar gray matter intensity.

(all as shown in Fig. 1) on the shortest echo time image. The mean signal magnitudes from each ROI in the MET$_2$ images were fitted to the sum of up to three decaying exponential functions, each with a Gaussian spectrum of log-spaced time constants, and a non-negative amplitude constraint (Stanisz and Henkelman, 1998). For each animal and ROI, the number of Gaussian-shaped T$_2$ components was determined by F-tests comparing χ^2 residuals between fits with 1, 2, or 3 components (Bevington and Robinson, 2003). Across all animals and ROIs, a k-means algorithm clustered the T$_2$ component values into short, intermediate, and long. For each animal and tract, the fraction of signal with short T$_2$ was defined as the MWF, consistent with previous definitions of this term (Mackay et al., 1994), and the fraction of the signal with long T$_2$ was defined analogously as the edema water fraction (EWF). Intra-ROI standard error in the EWF and MWF was estimated by voxel-by-voxel analysis of the MET$_2$ signal.

Since qMT images were acquired sequentially, images at all inversion-times were first rigidly co-registered (Viola and Wells, 1997). Because the qMT images were not exactly co-registered to the spin echo images, ROIs for qMT analysis were manually re-drawn to match the ROIs used in the MET$_2$ analysis. The mean signal magnitudes from each ROI were then fitted as a function of inversion time to a 5-parameter model describing longitudinal relaxation in a coupled two-pool model (Li et al., 2010). Three of these fitted parameters, T$_1$, the ratio of macromolecular pool size to free water pool size, defined here as the pool-size ratio (PSR), and an exchange rate (k_{mf}) were tabulated across all ROIs and rats. As above, intra-ROI standard error was estimated by voxel-by-voxel analysis of the qMT signal.

2.3. Histology and light microscopy

After MR imaging, three animals from each group were further processed for histological analysis. Animals were sacrificed by perfusion fixation—an initial flush of phosphate-buffered saline (PBS) was pushed directly into the left ventricle, followed by ≈15 min perfusion of a 4% glutaraldehyde and 0.5% paraformaldehyde in PBS. The cervical spinal cord was dissected, cut to ≈1 cm long segment surrounding the imaging slice and immersed in the same fixative solution for at least 48 h before being moved into PBS. Samples were post-fixed in 1% osmium tetroxide in cacodylate buffer, dehydrated in graded ethanol, and embedded in an epoxy resin. From each sample, a 1-μm thick section was cut axially from the middle of the embedded spinal cord sample (the approximate location of MRI measures) and stained with toluidine blue for evaluation by light microscopy. The thick sections of spinal cord were evaluated by light microscopy on an Olympus BX41 microscope equipped with an Optronics Microfire digital camera. A minimum of two histological images was collected from each of the aforementioned white matter tracts (dCST,

FG, RST and VST) and digitized into a 1600 × 1200 grid over a 120 × 90 μm^2 field of view.

Histological images were digitally smoothed with an edge-preserving anisotropic diffusion filter, enhanced with adaptive histogram equalization, and semi-automatically segmented using a region growing routine into regions of myelin (my), edema (ed), and intra/extra-axonal space (ie). For each tract, the segmented histology was used to tabulate the volume fraction, V, of each compartment. Then, with literature values for relative water density within each compartment (van der Knaap et al., 2005), ($\rho_{my} = 0.4$, $\rho_{ie} = 0.8$, $\rho_{ed} = 1.0$), the estimated water content fraction was defined as

$$W = V_{my}\rho_{my} + V_{ie}\rho_{ie} + V_{ed}\rho_{ed}, \tag{1}$$

and for each compartment was defined as

$$W_x = \frac{V_x\rho_x}{W} \tag{2}$$

where subscript "x" represents either myelin, intra/extra-axonal space, or edema. In addition, the number and area of individual lesions were tabulated, which provided estimates of mean lesion density and mean lesion diameter (computed from area based on a circular geometry).

3. Results

Representative T$_2$-weighted spin-echo images (echo time = 88.4 ms) are shown in Fig. 1 for both control and HCP600 rats, where images have been median-filtered and scaled to similar gray matter brightness. The white matter hyper-intensity in the images from the HCP600 rats relative to control rats suggests the presence of longer-lived T$_2$ signals, and these signals are apparent in the T$_2$ spectra from the two HCP groups, as shown in Fig. 2. Normal white matter is typically characterized by two T$_2$ components (Stewart et al., 1993), as found in the control animals, but the HCP-fed rats exhibited a third T$_2$ component (T$_2$ > 100 ms), defined here as the edema water component, with the signal fraction that increased with the severity of HCP intoxication. This increased EWF with HCP intoxication is presented in Fig. 3, which shows mean ± inter-animal standard deviation (SD) values of PSR, T$_1$, k_{mf}, MWF, and EWF for each tract and diet group. Small but statistically significant decreases in PSR and MWF and increases in T$_1$ were also observed between control and HCP intoxicated rats. There were no statistical differences in k_{mf} between groups.

Example histology and segmented histology from the dCST and VST tracts in control and HCP fed rats are shown in Fig. 4. The cross-sectional
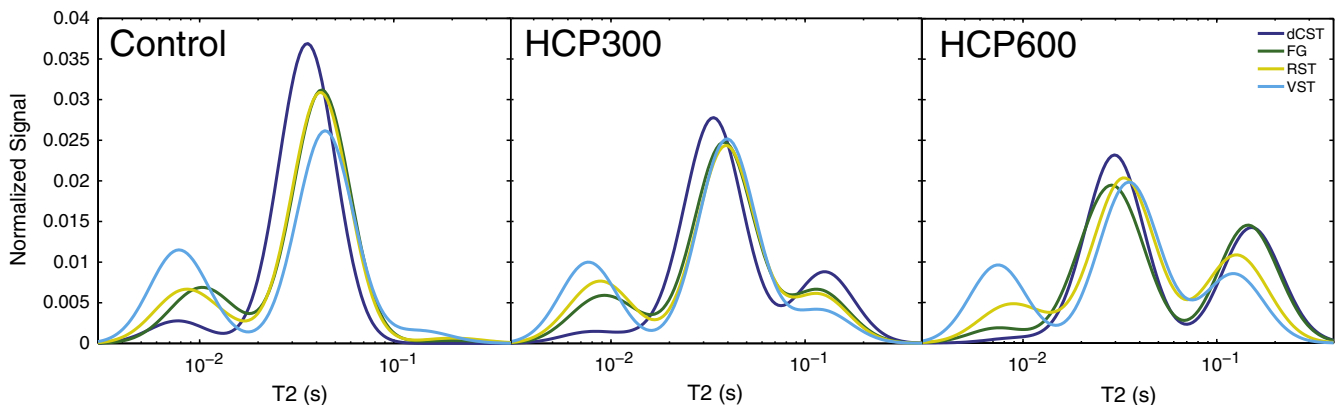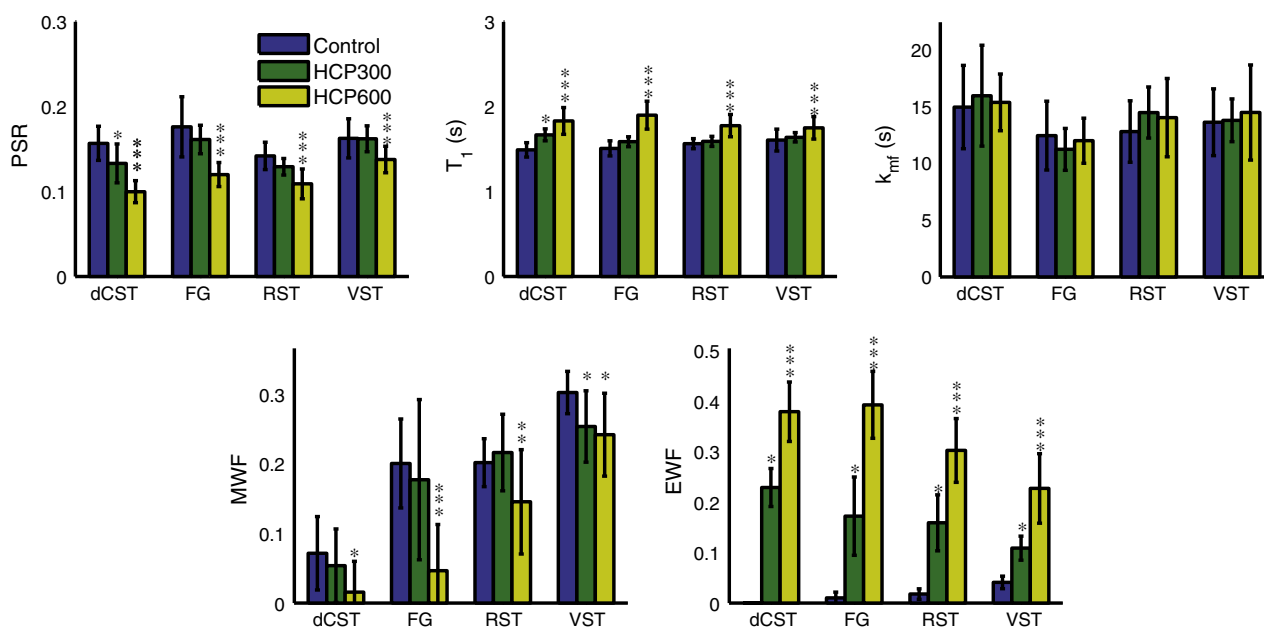

Fig. 2. Normalized T$_2$ spectra averaged across animals in the three groups—control, HCP300 and HCP600. A third T$_2$ component is a result of HCP intoxication, and the signal fraction increases with the level of intoxication.

Fig. 3. MR imaging metrics: pool size ratio (PSR), T_1 relaxation time-constant, macromolecular exchange rate (k_{mf}), myelin water fraction (MWF), and edema water fraction (EWF) in four spinal cord tracts of the spinal cord in all eight rats from each of the control, HCP300 and HCP600 groups. Error bars indicate inter-animal standard deviation. Asterisks indicate: * HCP300 or HCP600 is statistically significant ($P < 0.05$) compared to control, ** HCP600 is statistically significant ($P < 0.05$) compared to HCP300, and *** HCP600 is statistically significant ($P < 0.05$) compared to control and HCP300.

area of analyzed histology for each rat and tract represents $\approx 12\%$ of the mean ROI cross-sectional area analyzed with MRI. Red asterisks identify some occurrences of IME, characteristic of HCP intoxication. Across all tracts in both HCP300 and HCP600 animals, IME lesions exhibited a circular shape with diameter mean $\pm$ SD = 3.1 $\pm$ 0.4 μm. There was no statistical difference ($P < 0.05$) in average lesion diameter between tracts or HCP dose; however, the average lesion density (mean $\pm$ SD number of lesions per square mm) present was greater in HCP600 (1651 $\pm$ 201, 1291 $\pm$ 286, 545 $\pm$ 162, and 497 $\pm$ 150 in the dCST, FG, RST and VST respectively) compared to HCP300 (776 $\pm$ 97, 469 $\pm$ 345, 344 $\pm$ 178, and 142 $\pm$ 50 in the same tracts) in every tract ($P < 0.05$). The mean $\pm$ inter-animal SD of histology-derived water content fraction (W) as well as compartment specific myelin and edema water content fractions (W_{my} and W_{ed}, respectively) are shown in Fig. 5. In accord with the MRI observations of EWF, MWF and PSR, the histology showed large increases in W_{ed} in all tracts of HCP300 and HCP600 animals, and relatively small or insignificant changes in W and W_{my}.

The relationships between MRI metrics and histology are further shown in Figs. 6 & 7. Individual points are plotted for each tract and rat from which both MRI and histology metrics were available ($\pm$ intra-ROI standard error, as determined by voxel-by-voxel analysis). The lines show the best-fit linear relationship between MRI-derived and histology-derived metrics for data from individual tracts (colored according to the tract) and for all data (black). Fig. 6 shows significant correlations between EWF and W_{ed}, with a large overall coefficient of determination ($r^2 = 0.78$). However, this figure also shows that EWF overestimates W_{ed} by approximately a factor of 2× on average. In contrast, Fig. 7 shows only a weak correlation between MWF and W_{my} and no significant correlation between PSR and V_{my}.

4. Discussion

In this study, HCP was introduced into rat diets in order to alter the microstructure of white matter within the central nervous system. Parameters from MET_2 and qMT measurements were compared with quantitative evaluations of histology within several tracts within the spinal cord of normal and intoxicated rats to investigate the

specificity of these MRI metrics to variations in white matter microstructure. Compared with relatively unspecific contrast change in a T_2-weighted image, the use of MET_2 analysis demonstrated that the increased T_2 contrast was due to the addition of long T_2 signal, rather than the loss of short T_2 signal. Further, the significant correlation between the MRI- and histology-derived measures of edema, as shown in Fig. 6, demonstrates the utility of MET_2 measurements for quantitative evaluation of the severity of IME. These findings are in accord with and extend findings of several previous studies of water proton relaxation changes in experimental models of IME.

Spectroscopic experiments of excised rat white matter following triethyltin intoxication (Go and Edzes, 1975), known to cause IME, demonstrated correlations between mono-exponential measures of T_1 and T_2 with bulk water content, and observed the addition of a long T_2 component in white matter regions with IME lesions. Using similar methods, Naruse et al. also observed a bi-exponential T_2 in white matter with triethyltin-induced IME, and found a close correspondence between the time courses of the long T_2 value and the water content following intoxication (Naruse et al., 1982). Also, in peripheral nerve, IME resulting from dithiocarbamate intoxication has been associated with increased long-T_2 signals in spectroscopic studies (Valentine et al., 2007). Various preclinical imaging studies have also demonstrated the relationship between relaxation time constants and IME (Barnes et al., 1986, 1987; Jackson et al., 1994; Kinoshita et al., 2000; Lorenzo et al., 1989), and at least one study showed both an increased T_2 and signal fraction of long-T_2 signal from a bi-exponential T_2 analysis (Barnes et al., 1987).

Thus, there is a long-standing appreciation that IME will substantially alter water proton relaxation and generate the addition of a distinct long T_2 signal component, but the correlation of the size of this signal component to the volume fraction of edema has not previously been established. Fig. 6 demonstrates a significant correlation between the EWF, as measured by MET_2 MRI, and W_{ed}, the histological measure of edema water fraction, but it also shows that the EWF is consistently greater than W_{ed}. This mismatch cannot be simply explained by differential T_1 weighting on each T_2 signal component, because the edema water must have a longer T_1 than the rest of the tissue (as evidenced by the observed increases in bulk T_1 in HCP
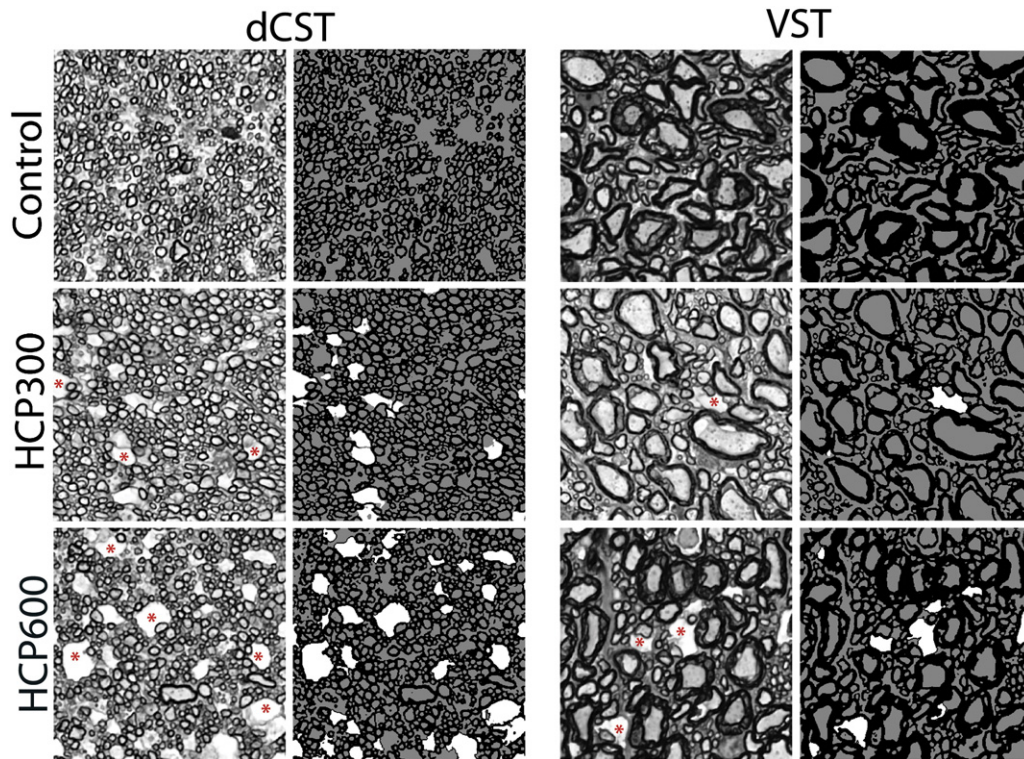
Fig. 4. Example histology from dCST and VST spinal cord tracts of control and HCP fed animals. FOV $= 30 \times 30~\mu m^2$. Red asterisks indicate a few regions of intramyelinic edema. The histology was segmented into regions of myelin (black), intra/extra-axonal space (gray), and intramyelinic edema (white).

rats), so T_1-weighting effects would result in a reduced, not increased estimate of EWF.

Alternatively, W_{ed} may have been systematically underestimated due to limitations of histological analysis. With any type of histological analysis, there is the risk of sampling bias due to the relatively small amount of tissue that can be examined, especially for cases where tissue changes appear in a few focal locations. For the case of HCP intoxication, lesions are known to be distributed diffusely within the spinal cord (Graham, 1989), so their density is not expected to vary substantially over the 1.5 mm thick MRI slice. Also, a relatively large areal fraction of the slice was analyzed by histology ($\approx 12\%$) so it is unlikely that particularly large lesions were systematically missed by histology across multiple animals. In addition to sampling error, the process of preparing tissue for histological analysis may alter compartment volumes. Extracellular volume can decrease during perfusion fixation, although this effect may also be reversed by post-fixing with osmium tetroxide (Van Harreveld and Khattab, 1968). Further, hard plastic embedding is known to cause a 2–4%

areal shrinkage of tissue (Oorschot et al., 1991; Tang and Nyengaard, 1997), which may manifest to a greater extent in regions of edema. It seems unlikely that these effects account for the factor of two differences between MRI and histological estimates of edema water, but the ultimate accuracy of the histological measures of compartment sizes is unknown.

Aside from systematic measurement errors, another factor that might explain the larger values of EWF compared with W_{ed} is the effect of inter-compartmental water exchange on the observed T_2 spectrum. The mathematical underpinning of exchange between two relaxing components is well established—as the rate of water exchange increases between two compartments, the amplitude of the faster-relaxing signal components diminishes, while the amplitude of the slower-relaxing component increases (Woessner, 1996; Zimmerman and Brittin, 1957). Thus, in the present case, water exchange between the vacuoles comprising the IME and the surrounding tissue will result in a long T_2 component with amplitude larger than the water volume fraction of all the vacuoles. The size of
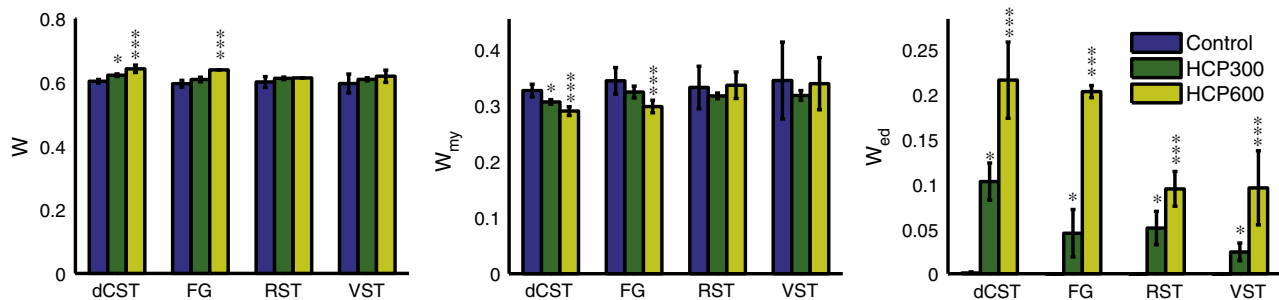
Fig. 5. Histology based water content (W), myelin water content fraction (W_{my}), and edema water content fraction (W_{ed}) in four spinal cord tracts of the spinal cord in three rats from each of the control, HCP300 and HCP600 groups. Error bars indicate inter-animal standard deviation determined from voxel-by-voxel analysis. Asterisks indicate: * HCP300 is statistically significant (P < 0.05) compared to control, *** HCP600 is statistically significant (P < 0.05) compared to control and HCP300.
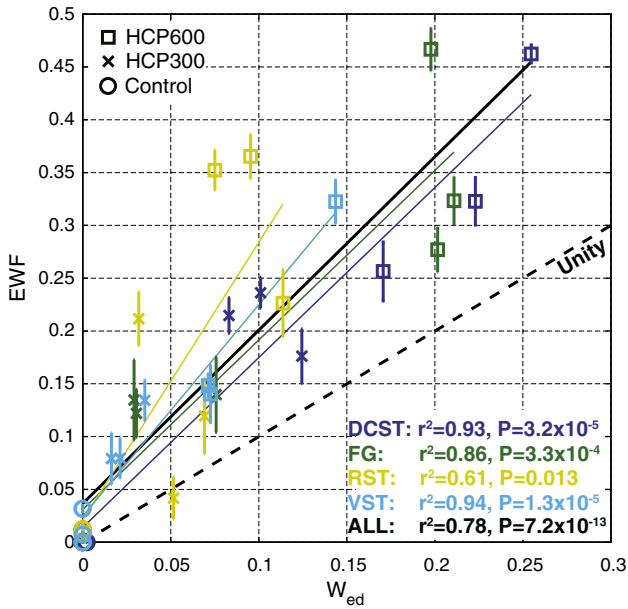
Fig. 6. Scatter plot comparing measures of edema water fraction from MET$_2$ imaging (EWF) with histology (W_{ed}) within four spinal cord tracts. Individual data points are plotted for animals for which both MRI and quantitative histology were obtained (3 per treatment group). Error bars indicate intra-ROI standard error, as estimated through voxel-by-voxel fitting. Solid lines draw linear regressions for individual tracts (colored to match the tract data points) as well as all tracks considered together (black, $r^2 = 0.78$).

vacuoles observed in this study (≈ 3 μm diameter) was small compared to the expected diffusion distance of free water over the transverse relaxation time of edema water, so it is reasonable to expect some effect of water exchange, but can this effect account for the EWF $\approx 2 \times W_{ed}$?

For simplicity, assume water exchanges only between the vacuoles and the intra/extra-axonal compartment space. Then consider a two-pool system with intrinsic $T_2s = 50$ ms and 150 ms, and 75% of the signal in the short T_2 pool, which roughly mimics the non-myelin water compartments observed in the HCP rats. With these numbers and the aforementioned mathematical descriptions of relaxation in two exchanging pools, it is easy to calculate that

with a residence time constant of the long-T_2 pool only as short as 200 ms, the observed transverse relaxation will be bi-exponential with two equally sized components. That is, the observed long T_2 component amplitude will be $2\times$ the size of the long-T_2 water pool volume fraction. Given the relatively small size of the vacuoles that comprise IME, a 200 ms residence time constant is not especially short, so these rough calculations indicate that water exchange is a plausible explanation for the two fold overestimation of W_{ed} by EWF.

While EWF proved a sensitive and relatively specific measure of IME, neither of the two more commonly studied probes of myelin – MWF or PSR – provided much insight into the micro-structural or -compositional changes resulting from HCP intoxication. Both MWF and PSR changed significantly due to HCP intoxication (Fig. 3), and these changes, if looked at in isolation, might be interpreted as due to decreases in myelin content. However, Fig. 5 demonstrates that there was little or no significant change in the myelin volume fraction due to HCP intoxication, nor was there an overall increase in water content which would result in reduced MWF and PSR by dilution. Unlike the case of interstitial edema, where water content increases and myelin volume fraction is displaced, the IME lesion formed at the expense of intra- and extra-axonal space, resulting in little or no changes in total water content change or myelin volume fraction.

The difference in the presentation of interstitial and intramyelinic edema is also illustrated in the studies of multiple sclerosis and phenylketonuria (Laule et al., 2007; Sirrs et al., 2007)—multiple sclerosis is known to cause interstitial edema, and is present in MET$_2$ analysis as a long T_2 component that is thought to vary in amplitude with the volume of interstitial water. In contrast, phenylketonuria, which is thought to result in IME lesions (Anderson and Leuzzi, 2010) produced consistent long T_2 signal fractions (Laule et al., 2007) and small but significant changes in water content (Sirrs et al., 2007).

A scatter plot of MWF vs W_{my} (Fig. 7, left) reveals a weak ($r^2 = 0.16$) but significant (P < 0.05) linear correlation, if all tracts and rats are considered. A previous study found much stronger correlation between MWF and histological measures of myelin content (Laule et al., 2006), which agreed with numerous prior qualitative evaluations (Does and Snyder, 1996; Moore et al., 2000; Odrobina et al., 2005; Stewart et al., 1993). However, all of those studies included comparison of normal tissues with demyelinated and/or non-myelinated tissues. The weaker correlation found here is likely due to the small range in myelin content within the spinal cord tracts analyzed, and consistent with previous studies of MWF in normal rat spinal cord (Dula et al., 2010; Harkins et
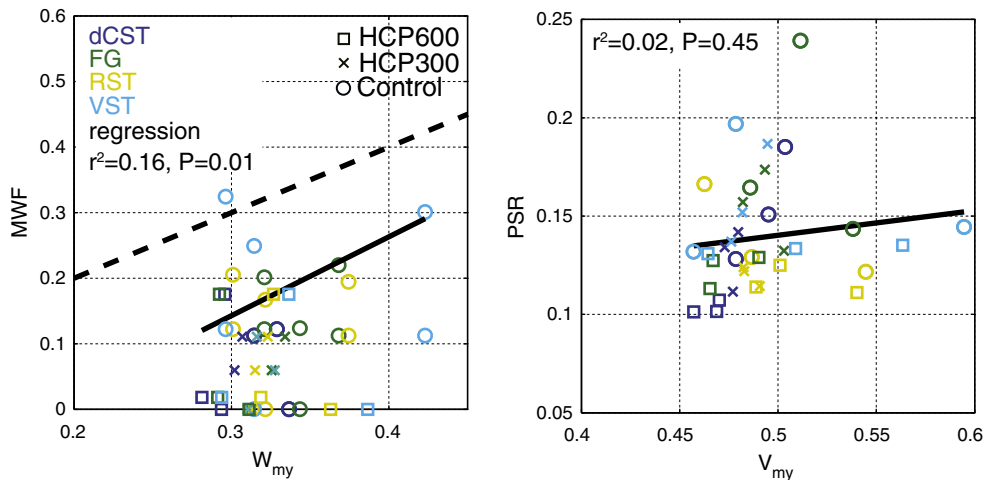
Fig. 7. Scatter plots comparing measures of myelin content from MRI and histology. On the left are plots of myelin water fraction from MET$_2$ imaging (MWF) vs histological estimates of myelin water volume fraction (W_{my}). On the right are plots of macromolecular pool size from qMT imaging (PSR) with histological measures of myelin volume fraction (V_{my}). Individual data points are plotted for animals for which both MRI and quantitative histology were obtained (3 per treatment group). Solid lines show best fit linear regressions for all data, which revealed a weak but significant correlation between MWF and W_{my} ($r^2 = 0.16$, P < 0.05) and no significant correlation between PSR and V_{my} ($r^2 = 0.02$, P > 0.05). The average intra-ROI standard error was small compared to the marker size, with average values of 0.016 for the MWF and 0.0051 for the PSR.

al., 2012) which showed wide variations in MWF across white matter tracts with similar myelin volume fractions. The MWF variation was postulated to result from variations in water exchange rate between myelin and non-myelin spaces. Similarly, in the present case, the formation of IME may result in more exchange of myelin water with long-T_2 water, which would then diminish the MWF. This effect would be greater in tracts with thinner myelin (dCST and FG), which agrees with the MWF observations shown in Fig. 3.

In contrast to MWF, no significant correlation was found between PSR and V_{my} ($r^2 = 0.02$, P > 0.4; Fig. 7, right). This observation is not surprising, given the relatively narrow range of myelin content changes resulting from HCP intoxication, and the fact that PSR is relatively insensitive to variations in the rate of water exchange between tissue compartments (Dula et al., 2010; Levesque and Pike, 2009). The cause of the small but significant decrease in PSR with HCP intoxication is not clear, but may reflect limits of a simple two-pool model of tissue (free water and macromolecules) to report on macromolecular content change when tissue water becomes heterogenous in T_1, as may be the case in with development of IME. Also, as postulated previously (Stanisz et al., 2004), PSR changes may reflect tissue pH changes, which has been shown to affect qMT measures in model myelin systems (Kucharczyk et al., 1994).

5. Conclusion

White matter lesions characterized by IME exhibit a long-T_2 signal component with amplitude (the EWF) that correlates with the severity of the IME, as measured histologically by the edema water volume fraction. However, much like MWF, EWF appears to be strongly affected by inter-compartmental water exchange, so care must be taken when interpreting results. Because the IME lesions in this study did not result in a substantial loss of myelin, previously established MRI reporters of myelin content, MWF (by MET_2) and PSR (by qMT) were not fully explained by changes in myelin content. Therefore, for characterizing white matter abnormalities where it is not known a priori that myelin loss is the primary lesion, such as those observed in pediatric patients taking vigabatrin, full T_2-spectral analysis, which provides measures of both myelin and edema contents, may be the most informative single protocol.

References

Aguilera-Albesa, S., Poretti, A., Honnef, D., Aktas, M., Yoldi-Petri, M.E., Huisman, T.A.G.M., Haeusler, M., 2012. T_2 hyperintense signal of the central tegmental tracts in children: disease or normal maturational process? Neuroradiology 54 (8), 863–871.
Anderson, P.J., Leuzzi, V., 2010. White matter pathology in phenylketonuria. Molecular Genetics and Metabolism 99, S3–S9.
Barnes, D., McDonald, W.I., Tofts, P.S., Johnson, G., Landon, D.N., 1986. Magnetic-resonance-imaging of experimental cerebral edema. Journal of Neurology, Neurosurgery, and Psychiatry 49 (12), 1341–1347.
Barnes, D., McDonald, W.I., Johnson, G., Tofts, P.S., Landon, D.N., 1987. Quantitative nuclear-magnetic-resonance imaging — characterization of experimental cerebral edema. Journal of Neurology, Neurosurgery, and Psychiatry 50 (2), 125–133.
Bevington, P.R., Robinson, D.K., 2003. Data Reduction and Error Analysis for the Physical Sciences, 3rd ed. McGraw-Hill Science 194–217.
Cammer, W., Rose, A.L., Norton, W.T., 1975. Biochemical and pathological-studies of myelin in hexachlorophene intoxication. Brain Research 98 (3), 547–559.
Carvlin, M.J., Asato, R., Hackney, D.B., Kassab, E., Joseph, P.M., 1989. High-resolution MR of the spinal-cord in humans and rats. American Journal of Neuroradiology 10 (1), 13–17.
Cohen, J.A., Fisher, R.S., Brigell, M.G., Peyster, R.G., Sze, G., 2000. The potential for vigabatrin-induced intramyelinic edema in humans. Epilepsia 41 (2), 148–157.

Dill, P., Datta, A.N., Weber, P., Schneider, J., 2013. Are vigabatrin induced T_2 hyperintensities in cranial MRI associated with acute encephalopathy and extrapyramidal symptoms? European Journal of Paediatric Neurology 17 (3), 311–315.
Does, M.D., Snyder, R.E., 1996. Multiexponential T_2 relaxation in degenerating peripheral nerve. Magnetic Resonance in Medicine 35 (2), 207–213.
Dortch, R.D., Harkins, K.D., Juttukonda, M.R., Gore, J.C., Does, M.D., 2012. Characterizing inter-compartmental water exchange in myelinated tissue using relaxation exchange spectroscopy. Magnetic Resonance in Medicine. http://dx.doi.org/10.1002/mrm.24571 (in press).
Dracopoulos, A., Widjaja, E., Raybaud, C., Westall, C.A., Snead, O.C., 2010. Vigabatrin-associated reversible MRI signal changes in patients with infantile spasms. Epilepsia 51 (7), 1297–1304.
Dula, A.N., Gochberg, D.F., Valentine, H.L., Valentine, W.M., Does, M.D., 2010. Multiexponential T_2, magnetization transfer, and quantitative histology in white matter tracts of rat spinal cord. Magnetic Resonance in Medicine 63 (4), 902–909.
Go, K.G., Edzes, H.T., 1975. Water in brain edema: observations by the pulsed nuclear magnetic resonance technique. Archives of Neurology 32 (7), 462–465.
Gochberg, D.F., Gore, J.C., 2007. Quantitative magnetization transfer imaging via selective inversion recovery with short repetition times. Magnetic Resonance in Medicine 57 (2), 437–441.
Graham, D., 1989. Neuropathology of vigabatrin. British Journal of Clinical Pharmacology 27, S43–S45.
Guo, J., Ji, Q., Reddick, W.E., 2012. Multi-slice myelin water imaging for practical clinical applications at 3.0 T. Magnetic Resonance in Medicine. http://dx.doi.org/10.1002/mrm.24527 (in press).
Harkins, K.D., Dula, A.N., Does, M.D., 2012. Effect of intercompartmental water exchange on the apparent myelin water fraction in multiexponential T_2 measurements of rat spinal cord. Magnetic Resonance in Medicine 67 (3), 793–800.
Jackson, G.D., Williams, S.R., Weller, R.O., van Bruggen, N., Preece, N.E., Williams, S., Butler, W.H., Duncan, J.S., 1994. Vigabatrin-induced lesions in the rat-brain demonstrated by quantitative magnetic-resonance-imaging. Epilepsy Research 18 (1), 57–66.
Karaarslan, E., Arslan, A., 2008. Diffusion weighted MR imaging in non-infarct lesions of the brain. European Journal of Radiology 65 (3), 402–416.
Kennedy, G.L., Gordon, D.E., 1976. Histopathologic changes produced by hexachlorophene in rat as a function of both magnitude and number of doses. Bulletin of Environmental Contamination and Toxicology 16 (4), 464–468.
Kimbrough, R.D., Gaines, T.B., 1971. Hexachlorophene effects on the rat brain: study of high doses by light and electron microscopy. Archives of Environmental Health 23 (3), 114–118.
Kinoshita, Y., Matsumura, H., Igisu, H., Yokota, A., 2000. Hexachlorophene-induced brain edema in rat observed by proton magnetic resonance. Brain Research 873 (1), 127–130.
Kucharczyk, W., Macdonald, P.M., Stanisz, G.J., Henkelman, R.M., 1994. Relaxivity and magnetization-transfer of white-matter lipids at MR-imaging — importance of cerebrosides and pH. Radiology 192 (2), 521–529.
Lampert, P., OBrien, J., Garrett, R., 1973. Hexachlorophene encephalopathy. Acta Neuropathologica 23 (4), 326–333.
Laule, C., Vavasour, I.M., Moore, G., Oger, J., Li, D., Paty, D.W., Mackay, A.L., 2004. Water content and myelin water fraction in multiple sclerosis — a T-2 relaxation study. Journal of Neurology 251 (3), 284–293.
Laule, C., Leung, E., Li, D.K.B., Troboulsee, A.L., Paty, D.W., Mackay, A.L., Moore, G.R.W., 2006. Myelin water imaging in multiple sclerosis: quantitative correlations with histopathology. Multiple Sclerosis 12 (6), 747–753.
Laule, C., Vavasour, I.M., Maedler, B., Kolind, S.H., Sirrs, S.M., Brief, E.E., Traboulsee, A.L., Moore, G.R.W., Li, D.K.B., Mackay, A.L., 2007. MR evidence of long T-2 water in pathological white matter. Journal of Magnetic Resonance Imaging 26 (4), 1117–1121.
Lebel, R.M., Wilman, A.H., 2010. Transverse relaxometry with stimulated echo compensation. Magnetic Resonance in Medicine 64 (4), 1005–1014.
Levesque, I.R., Pike, G.B., 2009. Characterizing healthy and diseased white matter using quantitative magnetization transfer and multicomponent T-2 relaxometry: a unified view via a four-pool model. Magnetic Resonance in Medicine 62 (6), 1487–1496.
Li, K., Zu, Z., Xu, J., Janve, V.A., Gore, J.C., Does, M.D., Gochberg, D.F., 2010. Optimized inversion recovery sequences for quantitative T(1) and magnetization transfer imaging. Magnetic Resonance in Medicine 64 (2), 491–500.
Lorenzo, A.V., Jolesz, F.A., Wallman, J.K., Ruenzel, P.W., 1989. Proton magnetic-resonance studies of triethyltin-induced edema during perinatal brain-development in rabbits. Journal of Neurosurgery 70 (3), 432–440.
Mackay, A.L., Whittall, K., Adler, J., Li, D., Paty, D., Graeb, D., 1994. In-vivo visualization of myelin water in brain by magnetic-resonance. Magnetic Resonance in Medicine 31 (6), 673–677.
Menon, R.S., Rusinko, M.S., Allen, P.S., 1992. Proton relaxation studies of water compartmentalization in a model neurological system. Magnetic Resonance in Medicine 28 (2), 264–274.
Moore, G.R.W., Leung, E., Mackay, A.L., Vavasour, I.M., Whittall, K.P., Cover, K.S., Li, D.K.B., Hashimoto, S.A., Oger, J., Sprinkle, T.J., Paty, D.W., 2000. A pathology-MRI study of the short-T_2 component in formalin-fixed multiple sclerosis brain. Neurology 55 (10), 1506–1510.
Narayana, P., Fenyes, D., Zacharopoulos, N., 1999. In vivo relaxation times of gray matter and white matter in spinal cord. Magnetic Resonance Imaging 17 (4), 623–626.
Naruse, S., Horikawa, Y., Tanaka, C., Hirakawa, K., Nishikawa, H., Yoshizaki, K., 1982. Proton nuclear magnetic-resonance studies on brain edema. Journal of Neurosurgery 56 (6), 747–752.
Odrobina, E., Lam, T.Y.J., Pun, T., Midha, R., Stanisz, G.J., 2005. MR properties of excised neural tissue following experimentally induced demyelination. NMR in Biomedicine 18 (5), 277–284.

Oorschot, D.E., Peterson, D.A., Jones, D.G., 1991. Neurite growth from, and neuronal survival within, cultured explants of the nervous system: a critical review of morphometric and stereological methods, and suggestions for the future. Progress in Neurobiology 37 (6), 525–546.

Ou, X., Sun, S.-W., Liang, H.-F., Song, S.-K., Gochberg, D.F., 2009. Quantitative magnetization transfer measured pool-size ratio reflects optic nerve myelin content in ex vivo mice. Magnetic Resonance in Medicine 61 (2), 364–371.

Pearl, P.L., Vezina, L.G., Saneto, R.P., McCarter, R., Molloy-Wells, E., Heffron, A., Trzcinski, S., McClintock, W.M., Conry, J.A., Elling, N.J., 2009. Cerebral MRI abnormalities associated with vigabatrin therapy. Epilepsia 50 (2), 184–194.

Prasloski, T., Maedler, B., Xiang, Q.-S., Mackay, A.L., Jones, C., 2012a. Applications of stimulated echo correction to multicomponent T_2 analysis. Magnetic Resonance in Medicine 67 (6), 1803–1814.

Prasloski, T., Rauscher, A., Mackay, A.L., Hodgson, M., Vavasour, I.M., Laule, C., Maedler, B., 2012b. Rapid whole cerebrum myelin water imaging using a 3D GRASE sequence. NeuroImage 63 (1), 533–539.

Righini, A., Ramenghi, L.A., Parini, R., Triulzi, F., Mosca, F., 2003. Water apparent diffusion coefficient and T_2 changes in the acute stage of maple syrup urine disease: evidence of intramyelinic and vasogenic–interstitial edema. Journal of Neuroimaging 13 (2), 162–165.

Simao, G.N., Mahmoodabadi, S.Z., Snead, O.C., Go, C., Widjaja, E., 2011. Abnormal axial diffusivity in the deep gray nuclei and dorsal brain stem in infantile spasm treated with vigabatrin. American Journal of Neuroradiology 32 (1), 199–203.

Sirrs, S.M., Laule, C., Madler, B., Brief, E.E., Tahir, S.A., Bishop, C., Mackay, A.L., 2007. Normal-appearing white matter in patients with phenylketonuria: water content, myelin water fraction, and metabolite concentrations. Radiology 242 (1), 236–243.

Sled, J.G., Pike, G.B., 2001. Quantitative imaging of magnetization transfer exchange and relaxation properties in vivo using MRI. Magnetic Resonance in Medicine 46 (5), 923–931.

Sled, J.G., Levesque, I., Santos, A.C., Francis, S.J., Narayanan, S., Brass, S.D., Arnold, D.L., Pike, G.B., 2004. Regional variations in normal brain shown by quantitative magnetization transfer imaging. Magnetic Resonance in Medicine 51 (2), 299–303.

Smith, S.A., Farrell, J.A.D., Jones, C.K., Reich, D.S., Calabresi, P.A., van Zijl, P.C.M., 2006. Pulsed magnetization transfer imaging with body coil transmission at 3 Tesla: feasibility and application. Magnetic Resonance in Medicine 56 (4), 866–875.

Stanisz, G.J., Henkelman, R.M., 1998. Diffusional anisotropy of T_2 components in bovine optic nerve. Magnetic Resonance in Medicine 40 (3), 405–410.

Stanisz, G.J., Midha, R., Munro, C.A., Henkelman, R.M., 2001. MR properties of rat sciatic nerve following trauma. Magnetic Resonance in Medicine 45 (3), 415–420.

Stanisz, J., Webb, S., Munro, C.A., Pun, T., Midha, R., 2004. MR properties of excised neural tissue following experimentally induced inflammation. Magnetic Resonance in Medicine 51 (3), 473–479.

Stewart, W.A., Mackay, A.L., Whittall, K.P., Moore, G., Paty, D.W., 1993. Spin–spin relaxation in experimental allergic encephalomyelitis — analysis of CPMG data using a nonlinear least-squares method and linear inverse-theory. Magnetic Resonance in Medicine 29 (6), 767–775.

Tang, Y., Nyengaard, J.R., 1997. A stereological method for estimating the total length and size of myelin fibers in human brain white matter. Journal of Neuroscience Methods 73 (2), 193–200.

Tozer, D.J., Davies, G.R., Altmann, D.R., Miller, D.H., Tofts, P.S., 2005. Correlation of apparent myelin measures obtained in multiple sclerosis patients and controls from magnetization transfer and multicompartmental T-2 analysis. Magnetic Resonance in Medicine 53 (6), 1415–1422.

Valentine, H.L., Does, M.D., Marshall, V., Tonkin, E.G., Valentine, W.M., 2007. Multicomponent T-2 analysis of dithiocarbamate-mediated peripheral nerve demyelination. Neurotoxicology 28 (3), 645–654.

van der Knaap, M.S., Valk, J., Barkhof, F., 2005. Magnetic Resonance of Myelination and Myelin Disorders. Springer, Berlin 7.

Van Harreveld, A., Khattab, F.I., 1968. Perfusion fixation with glutaraldehyde and post-fixation with osmium tetroxide for electron microscopy. Journal of Cell Science 3 (4), 579–594.

Vasilescu, V., Katona, E., Simplaceanu, V., Demco, D., 1978. Water compartments in the myelinated nerve. III. Pulsed NMR result. Experientia 34 (11), 1443–1444.

Viola, P., Wells, W.M., 1997. Alignment by maximization of mutual information. International Journal of Computer Vision 24 (2), 137–154.

Woessner, D.E., 1996. Brownian motion and its effects in NMR chemical exchange and relaxation in liquids. Concepts in Magnetic Resonance 8 (6), 397–421.

Yarnykh, V.L., 2002. Pulsed Z-spectroscopic imaging of cross-relaxation parameters in tissues for human MRI: theory and clinical applications. Magnetic Resonance in Medicine 47 (5), 929–939.

Zimmerman, J.R., Brittin, W.E., 1957. Nuclear magnetic resonance studies in multiple phase systems: lifetime of a water molecule in an absorbing phase on silica gel. The Journal of Physical Chemistry 61 (10), 1328–1333.